Powder Technology 387 (2021) 72–79

Contents lists available at ScienceDirect

Powder Technology

journal homepage: www.elsevier.com/locate/powtec

Compression of surface-wetted carbon-microsphere-based disks

Yulin Zhang, Fuqian Yang *

Materials Program, Department of Chemical and Materials Engineering, University of Kentucky, Lexington, KY 40506, United States of America

ARTICLE INFO

Article history:
Received 14 November 2020
Received in revised form 18 March 2021
Accepted 9 April 2021
Available online xxxx

Keywords:
Carbon microspheres
Wetting
Compression
Elastic modulus

ABSTRACT

Using hydrothermal process, we prepare carbon microspheres from fructose corn syrup and study the compression behavior of wetted carbon-based disks, which are made from carbon microspheres and polytetrafluoroethylene at a weight ratio of 4:1 and resembled to the carbon-based electrodes used in carbon-based supercapacitors. The migration/penetration of water into the disks is controlled by the placing time of water droplets on the top surface of the disks. The compressive behavior of the wetted carbon-based disks exhibits statistical variability, which is well described by the three-parameter Weibull probability distribution. Th calculated average elastic modulus decreases with the increase of the placing time of water droplets and with the decrease of the compressive stress. The correlation between the compressive stress and the average maximum strain follows a power-law relation with a power index in a range of 1.45 to 1.56.

1. Introduction

Carbon particles have been extensively used as electrode materials in the devices and systems for energy storage, including lithium-ion battery [1–3] and supercapacitor [4–7]. During electrochemical cycling, there exist ionic diffusion on the surface of carbon particles and/or intercalation/de-intercalation of ions/atoms in carbon particles, which can cause the deformation of the carbon particles [8–12]. The cycling-induced deformation has imposed a great concern to the structural durability of the carbon-based energy devices and systems, which requires the understanding of the mechanical behavior of carbon particles in the form of an individual particle and an "aggregate".

Tan and Li-Oakey [13] reported the dependence of the electrochemical performance of carbon fibers on the pore area/volume. Ali et al. [14] revealed that the structure of carbon materials plays an important role in determining the energy storage in supercapacitors. Masarapu et al. [15] found the increase of the specific capacitance of the supercapacitors made from carbon fibers with the increase of compression. Sun et al. [16] observed that the specific capacitance of the supercapacitors made from xylose-derived activated carbon increased nonlinearly with the increase of compressive stress. These results demonstrate the roles of the structure/aggregate and mechanical deformation of carbon materials in determining the performance of carbon-based supercapacitors.

Currently, there are limited studies focusing on the deformation of carbon particles/spheres. Yang et al. [17] performed compression test of individual core-shell nanospheres with an amorphous core on a transmission electron microscope (TEM) under a large compressive stress. They observed the collapse of inner pores and the buckling and twisting of the inner pore structures. Alazem et al. [18] studied the indentation deformation of the "cluster" of carbon nanospheres and obtained an average contact modulus of 16.6 GPa. Using nanoindentation, Zhu et al. [19] determined the contact modulus of a thin film made from hollow carbon spheres and found the contact modulus of a thin film was less than the contact modulus of individual hollow carbon spheres. Such behavior can be attributed to the compaction effect of hollow carbon spheres on the deformation of the film. Sun et al. [20] investigated the indentation behavior of individual carbon microspheres and revealed the decrease of contact modulus with the increase of indentation deformation.

In contrast to the study of the deformation of carbon particles/spheres, there are extensive studies on the compression of powder and water-saturated materials. Wünsch et al. [21] performed the compression of pharmaceutical powders, including microcrystalline cellulose, anhydrous lactose, anhydrous dicalcium phosphate and paracetamol, and revealed the decrease of porosity with the increase of compressive stress. However, the elastic analysis used by Wünsch et al. [21] is dubious since the effect of compaction needs to be included in the analysis. Frenning et al. [22] used a spring-network model to develop an effective-medium theory for the analysis of the pressure-strain relationship for the confined compression of microcrystalline cellulose. They did not address the inelastic deformation, which likely occurred during the compression of the microcrystalline cellulose. Kawakita and Lüdde [23] reviewed the relations between pressure and porosity and pointed out the importance of the change in the probability of particle orientation. All the results reveal that the compression of powders leads to the compaction/consolidation and the increase of mechanical

* Corresponding author.
E-mail address: fuqian.yang@uky.edu (F. Yang).

https://doi.org/10.1016/j.powtec.2021.04.024
0032-5910/

contact between powders, which can increase the nominal modulus/stiffness of consolidated materials. However, there are few studies on the effect of a water layer on the local compression of hydrophobic powders, especially carbon particles.

Considering the important applications of carbon particles/spheres in energy storage and their roles in controlling the structural durability of lithium-ion battery and supercapacitor, we study the compression deformation of carbon-microsphere-based disks, which are resembled to the carbon-based electrodes used in carbon-based supercapacitors. The focus is on the effects of wetted surface on the compression deformation of the carbon-microsphere-based disks. Prior to compression, a water droplet is placed on the surface of the carbon-microsphere-based disks to wet the disk surface for different times. The three-parameter Weibull probability distribution is used in the analysis of the compression deformation of the disks. The variations of the average elastic modulus of the disks and the average maximum compressive strain with the wetting time are discussed.

2. Experimental details

Using the method given by Cao and Yang [7], we prepared carbon microspheres via hydrothermal carbonization of a solution of fructose corn syrup (HFCS55, Cargill, Wayzata, MN). Briefly, the solution consisting of HFCS55, distilled (DI) water and 30 vol% sulfuric acid in a Teflon-lined autoclave was hydrothermally carbonized in an oven (THELCO, MODEL 19, Precision Scientific Company) at 493 K for 1 h. The solid powder formed in the autoclave was collected and placed in an oven at a temperature of 353 K to evaporate residual water for 12 h.

We performed the structure analysis of the formed carbon microspheres on an X-ray diffractometer (XRD) (Bruker D8, USA) and imaged the morphology of the formed carbon microspheres on a scanning electron microscope (SEM) (Hitachi S-4300, Japan). For the SEM imaging, a gold thin film was coated on the surface of the prepared solid powder at 2×10^{-6} mbar on a high vacuum coating machine (Leica ACE 600, Leica Microsystems Inc., US).

A mixture of the formed carbon microspheres and polytetrafluoroethylene (PTFE) powder (Spectrum Chemical MFG Corp, New Brunswick) in a weight ratio of 4:1 was prepared. After one-hour mixing in an agate mortar, the mixture was heated in air at 353 K for one hour to improve the binding between PTFE powder and carbon microspheres. The heat-treated mixture was air-cooled to room temperature. Carbon-microsphere-based disks were then prepared from the mixture under the action of 200 N in a compression machine (ESA-CU200, Shimadzu, Japan). The diameter and thickness of the disks were ~8 mm and 1.156 ± 0.026 mm, respectively. The mass of the disks was 5 ± 0.01 mg, and the porosity of the dicks was ~61%.

The local compression tests were conducted at ambient temperature on a Micro-Combi Tester (CSM Instrument, Needham, MA). Prior to the compression test, a droplet of DI water of 5 μl was placed on the surface of a carbon-microsphere-based disk in a closed chamber for a period of time in a range of 5 to 60 min to allow for the penetration of water into the disk. Fig. 1 shows optical images of a water droplet on the surface of a carbon-microsphere-based disk, which was placed on the surface of a PDMS (Polydimethylsiloxane) substrate. For comparison, a water droplet was also placed on the surface of a PDMS substrate simultaneously. According to Fig. 1, there is no significant change in the droplet size over the time, suggesting limited penetration of water to the carbon-microsphere-based disks.

The carbon-microsphere-based disk with the water droplet placed on top surface for a given time period was removed from the closed chamber and immediately placed on a stainless steel substrate under a Micro-Combi Tester (CSM Instrument, Needham, MA) for the compression test. A flat-ended, cylindrical rod of ~1.932 ± 0.001 mm in diameter, which was made from tool steel, was used to compress the carbon-based disks. The load-control mode was used for the tests. Note that the ratio of the diameter of the flat-ended, cylindrical rod to the disk thickness is 1.932:1.156, indicating that it is reasonable to refer the test to as compression test. The large Young's modulus and mechanical strength of the stainless steel suggests that the stainless steel substrate can be treated as a rigid substrate in comparison to the carbon-microsphere-based disks. Prior to performing a compressive test, the cylindrical rod was moved first to the specimen surface to initiate the contact with the specimen with the contact force less than 1 mN. After the contact, the cylindrical rod was pushed onto the specimen to reach the pre-determined peak load at a pre-determined loading rate, remained in contact with the specimen at the peak load in a holding stage, and was then retracted from the specimen at a pre-determined unloading rate. The loading and unloading rates were 400 mN/min. The peak load for the compression tests was in a range of 50 to 325 mN. The holding time of the holding stage between the loading phase and the unloading phase ranged from 5 to 30 s for the peak load of 342.4 mN (compressive stress of 109 kPa). For other compressive loads (stresses), the holding time was 10 s. Both the mechanical load

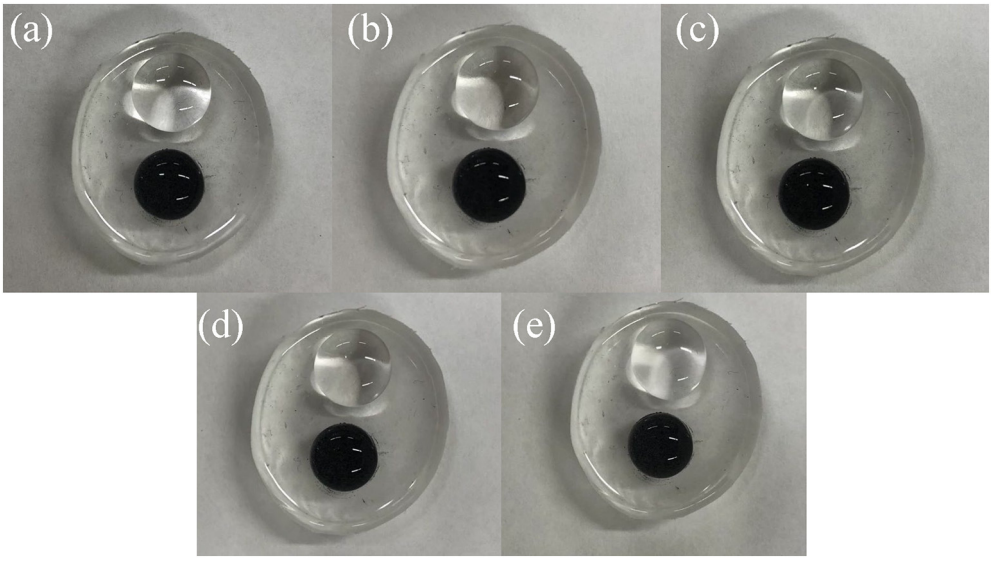

Fig. 1. Top view of aqueous droplets of 50 μl on the surfaces of PDMS and a carbon-microsphere-based disk at different instants: (a) 0 min, (b) 5 min, (c) 20 min, (d) 40 min and (e) 60 min. (The disk diameter is ~8 mm.)

and the rod displacement were recorded as functions of testing time. Ten different disks were tested for the same test conditions. Note that only one compression test was performed on each individual disk.

Following the procedure suggested by the CSM Instrument, we calibrated the Micro-Combi Tester with a test force of 300 mN and a calibration time of 30 min via microindentation of copper prior to the tests. The load-displacement curves were used in the calibration.

3. Results

The SEM images of the fructose-derived solid powder are presented in Fig. 2a-b. The fructose-derived solid powder are particles, and most of them are nearly spherical. Some particles are "welded" together. There is a neck connecting two joint particles. Such a structure is in consistence with the observation by Cao and Yang [7]. Using the SEM images, the average size of the fructose-derived solid spheres was found to be 6.33 ± 1.98 μm.

Fig. 3 depicts the powder XRD pattern of the fructose-derived solid spheres. There are two broad peaks centered at $2\theta = \sim 21.7°$ and ~ 43.2°. The strong broad peak at ~21.7° corresponds to (002) plane of amorphous carbon, suggesting that the fructose-derived solid spheres are amorphous [24,25]. The weak broad peak at ~43.2° corresponds to the (100) plane of the graphitic structure of carbon [26], revealing the graphitization of the fructose-derived solid spheres during the hydrothermal carbonization. The hydrothermal carbonization of the solution of fructose corn syrup led to the formation of amorphous carbon microspheres. From the XRD pattern, the degree of crystallinity of the fructose-derived carbon spheres is calculated to be 25.9%.

Fig. 4a presents the stress-strain curves for the compression of the carbon-microsphere-based disks under a peak compression stress of ~109 kPa with a holding period of 10 s and a placing time of 5 min for a water droplet. For the compression tests, the stress was calculated as the ratio of the applied force to the cross-section area of the rod, and the strain was calculated as the ratio of the change in the thickness to the initial thickness of the disk. There are three distinct stages: loading stage, holding stage and unloading stage. In the loading stage, the compressive strain increases with the increase of the compressive stress; in the unloading stage, the compressive strain decreases with the decrease of the compressive stress. From Fig. 4a, we note the scattering of the stress-strain curves, revealing the structure differences among the disks. Note that similar behavior has been observed for the compression test of porous materials [27].

Fig. 4b presents the stress-strain curves for the compression of the carbon-microsphere-based disks under different peak compression stresses with a holding period of 10 s and a placing time of 5 min for a water droplet. It is evident that increasing the peak stress increases the compressive deformation of the disks, as expected. The residual deformation, which is the strain difference between the separation point (zero force) in the unloading phase and the initial contact (zero strain), also increases with the increase in the peak stress.

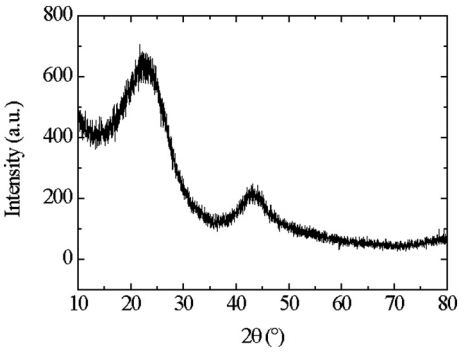

Fig. 3. XRD pattern of the fructose-derived solid spheres.

Fig. 4c shows the stress-strain curves for the compression of the carbon-microsphere-based disks under a peak compressive stress of 109 kPa with a holding period of 10 s for different placing times of water droplets. In general, increasing the placing time likely increases the compressive deformation of the disks due to that more water migrates into the disks to form a soft layer. All the results reveal the dependence of the compression deformation of the carbon-microsphere-based disks on the peak compressive stress and the placing time of a water droplet. Such a trend can be attributed to the presence of water in the disk due to the penetration of water into the disk. The water in the disk softens the disk and can reduce the resistance to the relatively sliding motion of adjacent carbon-microspheres, allowing large compressive strain to occur. The more the water in the disk, the larger is the thickness of the softened layer, and the larger is the compressive strain.

More stress-strain curves for the compression tests of the carbon-microsphere-based disks are given in Supplementary Information.

It is known that mechanical loading can cause the changes of the structures of porous materials and alter the mechanical responses of the porous materials. To characterize the effect of compression on the mechanical responses of the carbon-microsphere-based disks, we calculate the elastic modulus from unloading curves, which represents the elastic modulus of the compressed carbon-microsphere-based disks after the compression. The elastic modulus, E_n, of a compressed carbon-microsphere-based disk is calculated from the unloading stress-strain curve as

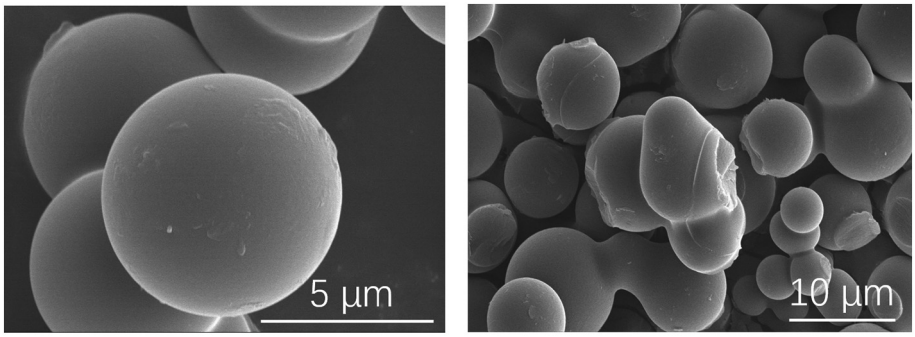

Fig. 2. a-b. SEM images of the fructose-derived solid powder.

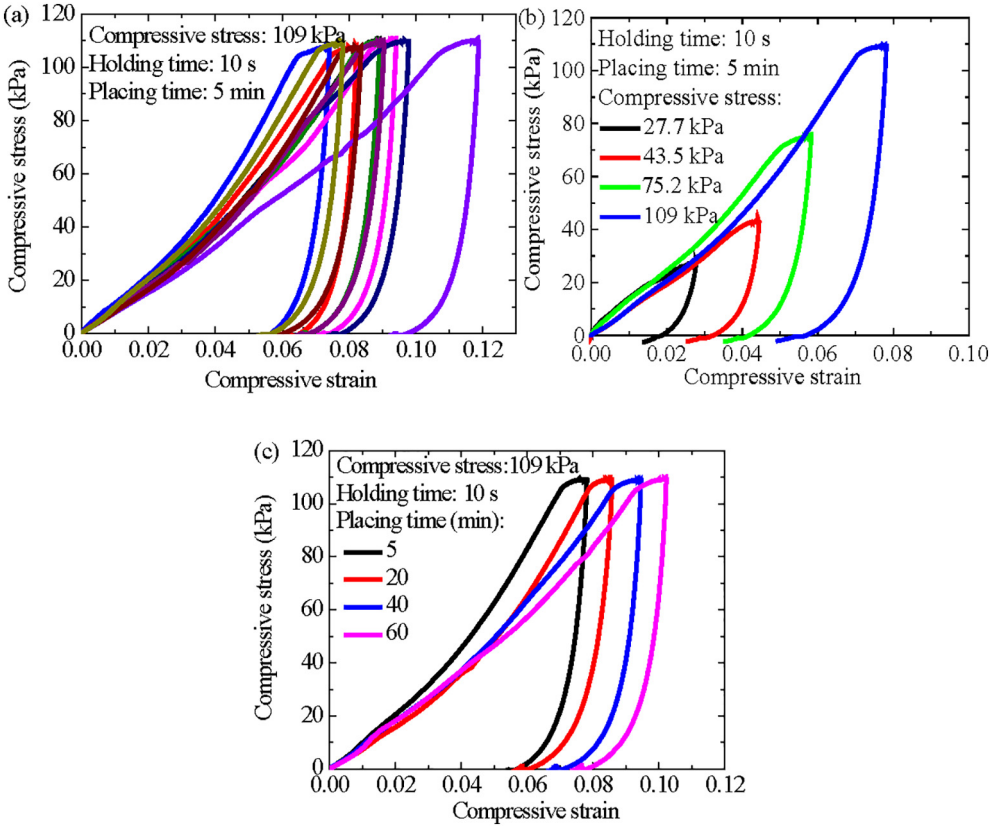

Fig. 4. Stress-strain curves for the compression of the carbon-microsphere-based disks with a holding period of 10 s: (a) under a compressive stress of 109 kPa with a placing time of 5 min for a water droplet, (b) under different compressive stresses with a placing time of 5 min for a water droplet, and (c) under a compressive stress of 109 kPa for different placing times of water droplets.

$$E_n = \frac{d\sigma}{d\varepsilon} = \frac{h}{\pi a^2}\frac{dF}{d\delta} \tag{1}$$

where σ is compressive stress, ε is compressive strain, h is the thickness of the disk, and a is the radius of the disk. F and δ are the load on the disk and the change of the disk thickness, respectively, during the unloading phase. Considering the nonlinear feature of the unloading curves, we follow the approach in nanoindentation and use the first 10% to 50% portion of unloading stress-strain curves to calculate the elastic modulus, E_n. Note that the stress in the first 10% to 50% portion of unloading stress-strain curves is an approximately linear function of strain.

Realizing the scattering characteristic of the stress-strain curves, as shown in Fig. 4a, a statistical method is needed to calculate the average elastic modulus of the compressed carbon-microsphere-based disks. There are reports that the Weibull distribution is suitable for the analysis of the mechanical responses of porous materials [27,28]. Here, we used the three-parameter Weibull distribution in the analysis of the mechanical responses of the carbon-microsphere-based disks. The three-parameter Weibull distribution for the event (property), x, is given as [29]

$$P(x) = 1 - \exp\left[-\left(\frac{x - x_{\min}}{x_0}\right)^n\right] \tag{2}$$

where $P(x)$ is the probability of the event (property), n is the Weibull modulus, and $x_{\min}$ denotes the threshold of the event (property). x_0 is a scale parameter of the event (property), at which the cumulative probability of the event ($x - x_{\min} = x_0$) is 63.2%. Using Eq. (2), the average value of the event (property), x_{mean}, can be calculated as [30].

$$x_{\text{mean}} = x_{\min} + x_0\Gamma\left(1 + n^{-1}\right) \tag{3}$$

where $\Gamma(\cdot)$ is the Gamma function.

Applying Eqs. (2) and (3) to the analysis of the elastic modulus of the compressed carbon-microsphere-based disks, we have

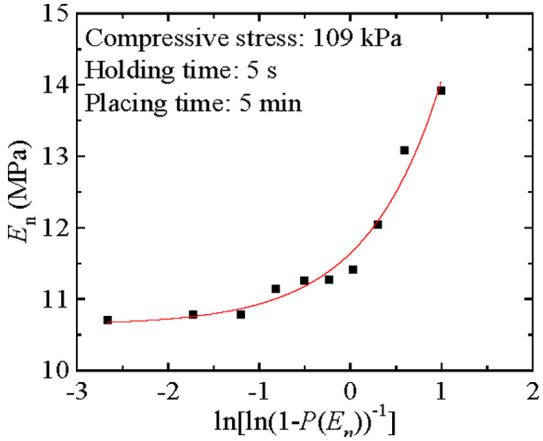

Fig. 5. Weibull distribution of the elastic modulus of the carbon-microsphere-based disks under the stress of 109 kPa with a holding time of 5 s and a placing time of 5 min for a water droplet.

$$P(E_n) = 1 - \exp\left[-\left(\frac{E_n - E_{\min}}{E_0}\right)^n\right] \text{ and } E_{\text{mean}} = E_{\min} + E_0\Gamma(1 + n^{-1}) \quad (4)$$

with $E_{\min}$, E_0, E_{mean} and n being the threshold, a scale parameter, average value and Weibull modulus of the elastic modulus of the carbon-microsphere-based disks, respectively.

Fig. 5 shows the distribution of the probability of the elastic modulus, E_n, determined from the unloading stress-strain curves for the compression of the carbon-microsphere-based disks under the compressive stress of 109 kPa with a holding time of 5 s and a placing time of 5 min for a water droplet. We used the first equation in Eq. (4) to fit the experimental results in Fig. 5 to obtain the numerical values of $E_{\min}$, E_0 and n for the elastic modulus of the carbon-microsphere-based disks. The fitting curve is represented by a solid red line in Fig. 5. In general, the three-parameter Weibull distribution can describe reasonably well the probability of the elastic modulus of the carbon-microsphere-based disks.

More results on the three-parameter Weibull distribution of the elastic modulus of the carbon-microsphere-based disks under different compressive stresses are given in Supplementary Information.

Using the fitting values of $E_{\min}$, E_0 and n and the second equation in Eq. (4), we calculated the average elastic modulus of the carbon-microsphere-based disks, E_{mean}, from the compression tests under different stresses with different holding times and placing times of water droplets. Fig. 6a presents the dependence of the average elastic modulus of the carbon-microsphere-based disks on the holding time for different placing times of water droplets under the compressive stress of 109 kPa. For the carbon-microsphere-based disks with wetted surface, the average elastic modulus increases first with the increase of the holding time and approaches plateau for the holding time larger than or equal to 20 s. Such a trend can be attributed to the compaction of the carbon-microsphere-based disks under compressive stress. Also, increasing the placing time of water droplets leads to the decrease of the average elastic modulus, suggesting the formation of a soft layer near the surface of the disk due to the migration of water into the disk.

Fig. 6b depicts the dependence of the average elastic modulus of the carbon-microsphere-based disks on the compressive stress for different placing times of water droplets with the holding time of 10 s. It is evident that increasing the compressive stress increases the average elastic modulus of the carbon-microsphere-based disks, revealing again the compaction of the disks during the compression.

For comparison, the average elastic moduli of the carbon-microsphere-based disks without wetted surface are also included in Fig. 6a-b. It is evident that the average elastic moduli of the carbon-microsphere-based disks without wetted surface are smaller than the corresponding ones. Such a trend is likely due to the presence of capillary force between adjacent carbon-microspheres, which is introduced by the penetration of water into the surface of the carbon-microsphere-based disks. The capillary force can increase the nominal strength of the disks.

Following the same approach, the three-parameter Weibull distribution was used to analyze the maximum compressive strain, $\varepsilon_{\max}$. Fig. 7a illustrates the distribution of the probability of the maximum compressive strain for the compression of the carbon-microsphere-based disks under the compressive stress of 109 kPa with the holding time of 5 s and the placing time of 5 min for water droplets. Using Eq. (2), we fit the results in Fig. 7a for the maximum compressive strain, $\varepsilon_{\max}$. The fitting curve is represented by the solid curve in Fig. 7a. In general, the probability distribution of the maximum compressive strain can be well described by the three-parameter Weibull distribution. Using the fitting results, we can calculate average maximum compressive strain for each set of testing conditions.

More results on the probability distribution of the maximum compressive strain for the carbon-microsphere-based disks with the fitting curves are given in Supplementary Information.

The variation of the average maximum compressive strain with the holding time for the compressive stress of 109 kPa with different placing times of water droplets is shown in Fig. 7b. There is no significant difference between the average maximum compressive strains of different holding times, revealing that the holding time in the range of 5 to 30 s had limited effect on the compressive behavior of the carbon-microsphere-based disks with water droplets placed on the surface. For the same holding time, the average maximum compressive strain generally increases with the increase of the placing time of water droplet. Such results suggest that the placing time of water droplet plays a more dominant role in the deformation of the carbon-microsphere-based disks with water droplets than the effect of the holding time.

The dependence of the average maximum compressive strain on the average maximum compressive stress is depicted in Fig. 7c for the compression tests with the holding time of 10 s and different placing times of water droplets. Increasing the compressive stress increases the average maximum compressive strain, as expected, for all the placing times of water droplets. Under the same compressive stresses, the average maximum compressive strain increases with the increase of the placing time of water droplet in accord with the results in Fig. 7b.

4. Discussion

According to Fig. 6b, the average elastic modulus of the carbon-microsphere-based disks decreases with the increase of the placing time of water droplets under the same compressive stress. Such behavior can be attributed to the effect of capillary force on the overall

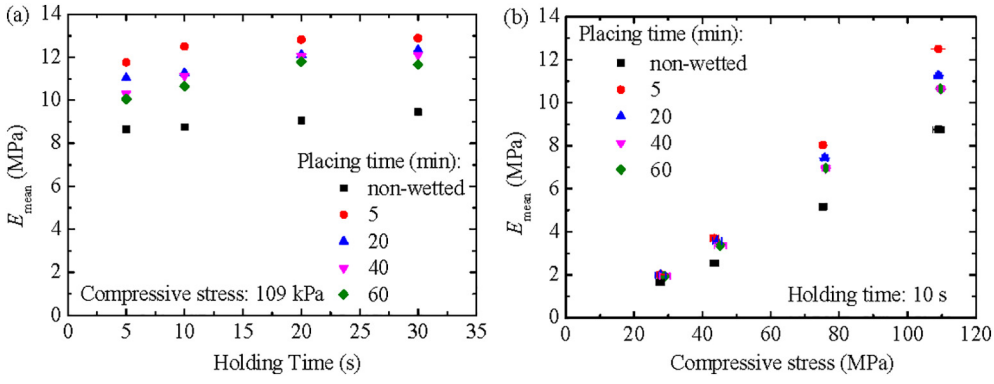

Fig. 6. (a) Dependence of the average elastic modulus of the carbon-microsphere-based disks on the holding time for different placing times of water droplets under the compressive stress of 109 kPa, and (b) dependence of the average elastic modulus of the carbon-microsphere-based disks on the compressive stress for different placing times of water droplets with the holding time of 10 s. For comparison, the average elastic moduli of the carbon-microsphere-based disks without wetted surface are also included in the figure.

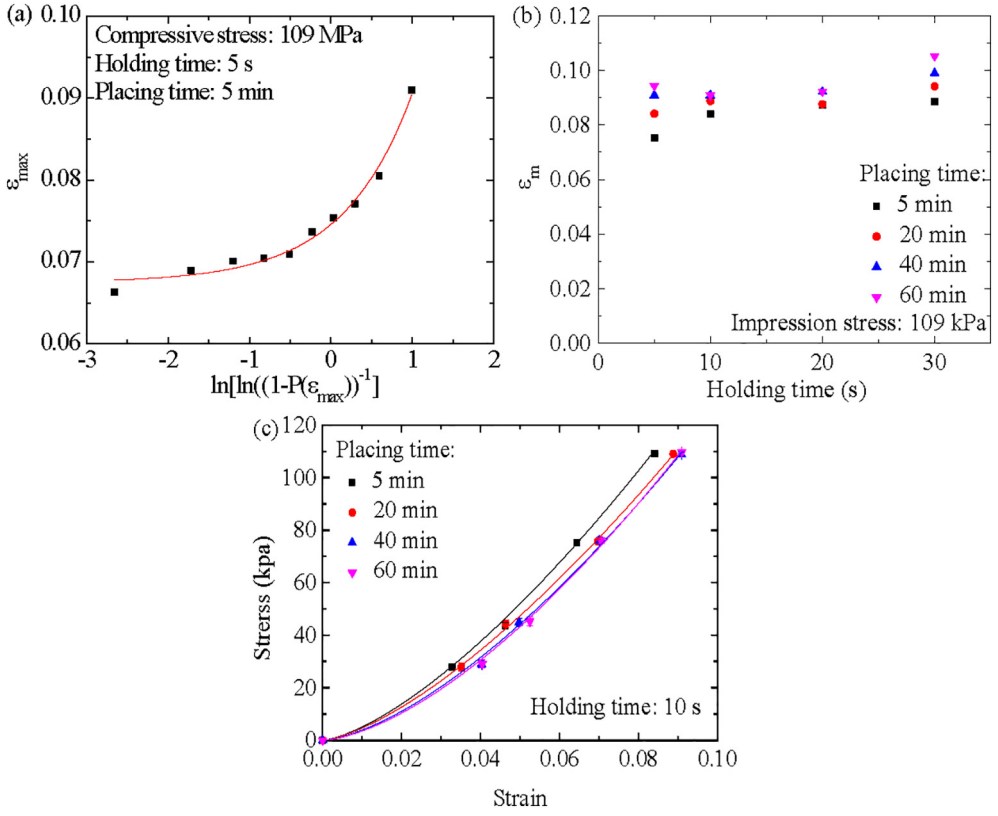

Fig. 7. (a) Probability distribution of the maximum compressive strain for the compression of the carbon-microsphere-based disks under the compressive stress of 109 kPa with the holding time of 5 s and the placing time of 5 min for water droplets, (b) variation of the average maximum compressive strain with the holding time for the compressive stress of 109 kPa with different placing times, and (c) variation of the average maximum compressive strain with the compressive stress for the holding time of 10 s with different placing times of water droplets.

elastic deformation of the carbon-microsphere-based disks. The negative pressure, which is generated by the water bridge between carbon microspheres, contributes to the effective stress on the water-rich layer in the carbon-microsphere-based disks and can cause the increase of the elastic modulus for un-saturated carbon-microsphere-based disks.

The effect of the effective stress on the mechanical behavior of the water-rich layer is dependent on the degree of saturation in the pore-space. It is known that the elastic modulus of the porous structures made from fine-grained cohesionless particles increases first with the increase of the degree of saturation, reaches maximum, and then decreases with the increase of the degree of saturation [31]. The decreasing trend of the elastic modulus of the carbon-microsphere-based disks with the placing time of water droplets for placing time larger than or equal to 20 min reveals the decrease of the effective stress in the water-rich layer due to the increase in the degree of saturation.

From Figs. 6b, we note that the average elastic modulus of the carbon-microsphere-based disks for the same placing time of water droplets is a linearly increasing function of the compressive stress. Such a trend can be attributed to the compaction of the carbon-microsphere-based disks under compressive stress. Increasing compressive stress increases the density of a porous material, leading to the increase in the elastic modulus of the porous material.

Using linear regression to fit the results in Fig. 6b, we obtained the increasing rate of the elastic modulus per unit stress, λ, in the unit of kPa/kPa. Fig. 8 displays the variation of the increasing rate of the elastic modulus per unit stress with the placing time. The smaller the placing time, the larger is the increasing rate of the elastic modulus per unit stress. This trend suggests that the thicker the water-rich layer, the larger is the resistance to the compaction of the carbon-microsphere-based disks. This is because the thickness of the water-poor layer decreases with the increase of the placing time of water droplets and a larger force is needed to cause the same degree of deformation of a thinner disk due to the substrate effect.

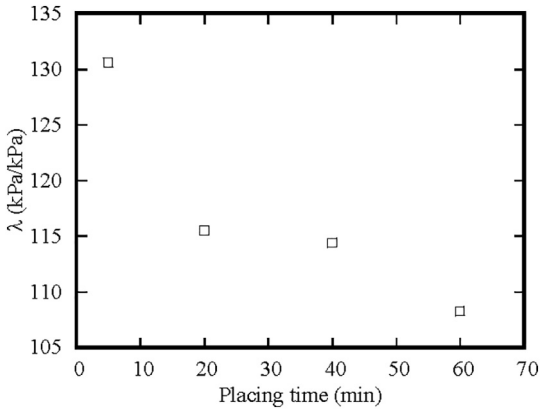

Fig. 8. Variation of the increasing rate of the elastic modulus per unit stress with the placing time.

According to Fig. 7c, there exists a nonlinear correlation between the compressive stress and the average maximum compressive strain, which is in accordance with Fig. 4. Assume that the nonlinear correlation between the compressive stress, σ, and the average maximum compressive strain, ε_m, follows a power-law relation as

$$\sigma = a\varepsilon_m^{n'} \quad (5)$$

where a is a pre-exponential factor and n' is a power index. Using Eq. (5) to curve-fit the results in Fig. 7c, we obtained (a, n') as (3984.40, 1.45), (3606.40, 1.45), (4155.26, 1.52) and (4684.04, 1.56) for the placing times of 5, 20, 40 and 60 min. For comparison, the fitting curves are also included in Fig. 7c. In general, there is no statistical difference between 1.45 and 1.56 for the compression of the carbon-microsphere-based disks with water-rich and water-poor layers. There is no change in the mechanisms controlling the compaction of the carbon-microsphere-based disks with water-rich and water-poor layers. The differences among the pre-exponential factors may reveal the effect of the placing time (penetration/flow) of water into the disks. The larger the placing time, the more is water into the disk, and the compliant is the disk.

The increase in the elastic modulus of the compressed carbon-microsphere-based disks with the increase of the compressive stress suggests that the compression of the carbon-based electrodes in electrolyte can increase the packing density, which can lead to the increase of electric conductivity and the improvement of the electrochemical performance of carbon-based supercapacitors, as supported by the results observed by Sun et al. [16]. Applying reasonable compressive stress can improve the structural integrity of the carbon-based electrode and improve the long-term stability of carbon-based supercapacitors.

5. Conclusion

The structural durability of the carbon-based lithium-ion battery and supercapacitor depends on the mechanical behavior and structural integrity of carbon-based electrode. Realizing the wide use of activated carbon in the devices and systems for energy storage, we have investigated the compressive behavior of the carbon-microsphere-based disks with water-rich and water-poor layers. The formation of the water-rich layer was controlled by the penetration/migration of water into the disks for different placing times of water droplets on the surface of the disks.

The results from the compression tests demonstrate the presence of the structure variations among the carbon-microsphere-based disks, suggesting that the particle-based electrode materials for lithium-ion battery and supercapacitor are inhomogeneous and disordered. The penetration/migration of water (liquid) can increase the interaction between adjacent carbon-microspheres through capillary force, which can lead to the increase in the nominal stiffness (modulus) of the carbon-microspheres-based materials. However, the water effect on the water-wetted layer is dependent on the degree of saturation in the pore-space.

The structural variation of the carbon-microsphere-based disks limits the use of deterministic method in the analysis of the mechanical behavior (elastic modulus) of the carbon-microsphere-based disks. The three-parameter Weibull distribution was used to analyze the deformation behavior of the carbon-microsphere-based disks with water-rich and water-poor layers and to calculate the average elastic modulus and average maximum compressive strain. There exists a power-law relationship between the compressive stress and the average compressive strain with a power index in a range of 1.45 to 1.56.

Data availability

The data supporting the findings of this study are included in Supplementary Information.

CRediT authorship contribution statement

Yulin Zhang: Experiment, Data curation, Writing - original draft.
Fuqian Yang: Conceptualization, Experimental design, Writing - review & editing, Supervision.

Declaration of Competing Interest

The authors declare that they have no known competing financial interests or personal relationships that could have appeared to influence the work reported in this paper.

Acknowledgement

FY is grateful for the support from the NSF [CMMI-1634540], monitored by Drs. Khershed Cooper and Thomas Francis Kuech.

Appendix A. Supplementary data

Supplementary data to this article can be found online at https://doi.org/10.1016/j.powtec.2021.04.024.

References

[1] Z. Chen, J. Ye, R. Qin, Q. Hao, C. Xu, J. Hou, Carbon particles modified macroporous Si/Ni composite as an advanced anode material for lithium ion batteries, Int. J. Hydrog. Energy 44 (2019) 1078–1087.
[2] Z. Jiang, J. Li, Y. Yang, L. Mu, C. Wei, X. Yu, P. Pianetta, K. Zhao, P. Cloetens, F. Lin, Machine-learning-revealed statistics of the particle-carbon/binder detachment in lithium-ion battery cathodes, Nat. Commun. 11 (2020) 1–9.
[3] L. Ao, C. Wu, Y. Xu, X. Wang, K. Jiang, L. Shang, Y. Li, J. Zhang, Z. Hu, J. Chu, A novel Sn particles coated composite of SnO_x/ZnO and N-doped carbon nanofibers as high-capacity and cycle-stable anode for lithium-ion batteries, J. Alloys Compd. 819 (2020) 153036.
[4] J. Wang, Q. Li, C. Peng, N. Shu, L. Niu, Y. Zhu, To increase electrochemical performance of electrode material by attaching activated carbon particles on reduced graphene oxide sheets for supercapacitor, J. Power Sources 450 (2020) 227611.
[5] A. Macías-García, D. Torrejón-Martín, M.Á. Díaz-Díez, J.P. Carrasco-Amador, Study of the influence of particle size of activate carbon for the manufacture of electrodes for supercapacitors, J. Ener. Stor. 25 (2019) 100829.
[6] S. Wang, W. Sun, D.-S. Yang, F. Yang, Conversion of soybean waste to sub-micron porous-hollow carbon spheres for supercapacitor via a reagent and template-free route, Mater. Today Ener. 13 (2019) 50–55.
[7] W. Cao, F. Yang, Supercapacitors from high fructose corn syrup-derived activated carbons, Mater. Today Ener. 9 (2018) 406–415.
[8] N. Li, D. Su, In-situ structural characterizations of electrochemical intercalation of graphite compounds, Carbon Ener. 1 (2019) 200–218.
[9] E. Jones, Ö. Çapraz, S. White, N. Sottos, Reversible and irreversible deformation mechanisms of composite graphite electrodes in lithium-ion batteries, J. Electrochem. Soc. 163 (2016) A1965.
[10] C. Sole, N.E. Drewett, L.J. Hardwick, In situ Raman study of lithium-ion intercalation into microcrystalline graphite, Faraday Discuss. 172 (2014) 223–237.
[11] R. Purkayastha, R. McMeeking, A parameter study of intercalation of lithium into storage particles in a lithium-ion battery, Comput. Mater. Sci. 80 (2013) 2–14.
[12] M.D. Levi, L. Daikhin, D. Aurbach, V. Presser, Quartz crystal microbalance with dissipation monitoring (EQCM-D) for in-situ studies of electrodes for supercapacitors and batteries: a mini-review, Electrochem. Commun. 67 (2016) 16–21.
[13] S. Tan, K.D. Li-Oakey, Effect of structural orientation on the performance of supercapacitor electrodes from electrospun coal-derived carbon nanofibers (CCNFs), J. Electrochem. Soc. 166 (2019) A3294.
[14] B.A. Ali, O.I. Metwalli, A.S. Khalil, N.K. Allam, Unveiling the effect of the structure of carbon material on the charge storage mechanism in MoS_2-based supercapacitors, ACS Omega 3 (2018) 16301–16308.
[15] C. Masarapu, L.-P. Wang, X. Li, B. Wei, Tailoring electrode/electrolyte interfacial properties in flexible supercapacitors by applying pressure, Adv. Energy Mater. 2 (2012) 546–552.
[16] W. Sun, Y. Zhang, F. Yang, Tuning electrochemical performance of carbon-sphere-based supercapacitors by compressive stress, Electrochim. Acta 357 (2020) 136874.
[17] W. Yang, S. Mao, J. Yang, T. Shang, H. Song, J. Mabon, W. Swiech, J.R. Vance, Z. Yue, S.J. Dillon, Large-deformation and high-strength amorphous porous carbon nanospheres, Sci. Rep. 6 (2016) 24187.
[18] A.A. Alazemi, A.D. Dysart, V.G. Pol, Experimental investigation of the mechanical and surface properties of sub-micron carbon spheres, Lubricants 8 (2020) 77.
[19] Z. Zhu, Z. Chen, G. Lin, Y. Ge, Y. Tu, H. Chen, S. Ye, X. Yang, Buckled amorphous hollow carbon spheres: facile fabrication, buckling process, and applications as

electrode materials for supercapacitors, ACS Appl. Mater. Interfaces 11 (2019) 30116–30124.
[20] Y. Sun, R. Chen, G. Zhao, F. Yang, Nanoindentation of carbon microspheres, Int. J. Mater. Res. 107 (2016) 687–691.
[21] I. Wunsch, J.H. Finke, E. John, M. Juhnke, A. Kwade, A mathematical approach to consider solid compressibility in the compression of pharmaceutical powders, Pharmaceutics 11 (2019) 121.
[22] G. Frenning, F. Mahmoodi, J. Nordström, G. Alderborn, An effective-medium analysis of confined compression of granular materials, Powder Technol. 194 (2009) 228–232.
[23] K. Kawakita, K.-H. Lüdde, Some considerations on powder compression equations, Powder Technol. 4 (1971) 61–68.
[24] V.A.A.T. Drits, Cyril, X-Ray diffraction by disordered lamellar structures, Springer-Verlag, New York, 1991.
[25] H. Shi, J.N. Reimers, J.R. Dahn, Structure-refinement program for disordered carbons, J. Appl. Crystallogr. 26 (1993) 827–836.
[26] A.M. Dehkhoda, A.H. West, N. Ellis, Biochar based solid acid catalyst for biodiesel production, Appl. Catalysis A 382 (2010) 197–204.
[27] A.Y. Smolin, G. Eremina, S.Y. Korostelev, Dependences of mechanical properties of ceramics with bimodal pore size distribution on the porosity at various scale levels, Russ. Phys. J. 62 (2019) 1445–1454.
[28] X. Shi, S. Jiang, S. Lu, Z. He, D. Li, Z. Wang, D. Xiao, Investigation of mechanical properties of bedded shale by nanoindentation tests: a case study on lower Silurian Longmaxi formation of Youyang area in Southeast Chongqing, China, Pet. Explor. Dev. 46 (2019) 163–172.
[29] W. Weibull, A statistical distribution function of wide applicability, J. Appl. Mech. 18 (1951) 293–297.
[30] C.V. Sia, Y. Nakai, D. Shiozawa, H. Ohtani, Statistical analysis of the tensile strength of treated oil palm fiber by utilisation of weibull distribution model, Open J. Comp. Mater. 4 (2014) 72–77.
[31] S. Wu, D.H. Gray, F. Richart Jr., Capillary effects on dynamic modulus of sands and silts, J. Geotech. Eng. 110 (1984) 1188–1203.